

Metal-mass-to-light ratios of the Perseus cluster out to the virial radius

K. Matsushita¹, E. Sakuma¹, T. Sasaki¹, K. Sato¹ and A. Simionescu²

ABSTRACT

We analyzed XMM-Newton data of the Perseus cluster out to ~ 1 Mpc, or approximately half the virial radius. Using the flux ratios of $\text{Ly}\alpha$ lines of H-like Si and S to $\text{K}\alpha$ line of He-like Fe, the abundance ratios of Si/Fe and S/Fe of the intracluster medium (ICM) were derived using the APEC plasma code v2.0.1. The temperature dependence of the line ratio limits the systematic uncertainty in the derived abundance ratio. The Si/Fe and S/Fe in the ICM of the Perseus cluster show no radial gradient. The emission-weighted averages of the Si/Fe and S/Fe ratios outside the cool core are 0.91 ± 0.08 and 0.93 ± 0.10 , respectively, in solar units according to the solar abundance table of Lodders (2003). These ratios indicate that most Fe was synthesized by supernovae Ia. We collected K -band luminosities of galaxies and calculated the ratio of Fe and Si mass in the ICM to K -band luminosity, iron-mass-to-light ratio (IMLR) and silicon-mass-to-light ratio (SMLR). Within ~ 1 Mpc, the cumulative IMLR and SMLR increase with radius. Using Suzaku data for the northwest and east directions, we also calculated the IMLR out to ~ 1.8 Mpc, or about the virial radius. We constrained the SMLR out to this radius and discussed the slope of the initial mass function of stars in the cluster. Using the cumulative IMLR profile, we discuss the past supernova Ia rate.

Subject headings: galaxies:clusters:individual(the Perseus cluster)– X-rays:intracluster medium

1. Introduction

Clusters of galaxies are the largest gravitationally bound objects in the Universe. The intracluster medium (ICM) contains a large amount of metals, synthesized by supernovae (SNe) in cluster galaxies. Thus, the distribution of metals in the ICM provides important information on the chemical history and evolution of clusters.

Because metals were synthesized in galaxies, the ratios of metal mass in the ICM to the total light from galaxies in clusters or groups, (i.e., metal-mass-to-light ratios) are key parameters in investigating the chemical evolution

of the ICM. Using Einstein and Ginga data, Arnaud et al. (1992) and Tsuru (1992) derived ratios of Fe mass in the ICM to the total light from galaxies, which is the iron-mass-to-light ratio (IMLR). To account for the observed IMLR, either the past average rate of SN Ia was at least higher by a factor of 10 than the present rate or massive stars in clusters formed with a very flat initial mass function (Renzini et al. 1993). With ASCA observations, the derived IMLR within a radius where the ICM density falls below $3 \times 10^{-4} \text{ cm}^{-3}$ is nearly constant in rich clusters and decreases toward poorer systems (Makishima et al. 2001). With Suzaku, Chandra, and XMM satellites, the IMLR of several medium-sized clusters and groups of galaxies was measured out to $0.2r_{180}$ – $0.5r_{180}$ (Matsushita et al. 2007a; Komiyama et al. 2009; Sato et al. 2007, 2008, 2009a,b, 2010; Rasmussen & Ponman 2009; Sakuma et al. 2011) and that of the Coma cluster was derived out to $0.5r_{180}$ (Matsushita et al.

¹Department of physics, Tokyo University of Science, 1-3 Kagurazaka, Shinjuku-ku, Tokyo 162-8601, Japan; matsumita@rs.kagu.tus.ac.jp

²KIPAC, Stanford University, 452 Lomita Mall, Stanford, CA 94305, USA

³Department of Physics, Stanford University, 382 Via Pueblo Mall, Stanford, CA 94305-4060, USA

2012). Suzaku first measured the Fe abundance of the ICM beyond $0.5r_{180}$ (Fujita et al. 2008; Simionescu et al. 2011). With Suzaku, Sato et al. (2012) derived the IMLR profile of the Hydra A cluster out to r_{180} . Here, r_{180} is the radius in which matter at 180 times the critical density of the universe is contained. In individual clusters, the IMLR is lower around the center, indicating that Fe in the ICM extends farther than stars. Therefore, to derive the total Fe mass in the ICM, we need observations out to the virial radius.

Since Fe is synthesized by both SNe Ia and by core-collapse SNe (hereafter SNecc), we need measurements of abundances of various elements to constrain contributions from the two types of SNe. The ASCA satellite first studied the Si abundance in the ICM (Fukazawa et al. 1998, 2000; Finoguenov et al. 2000, 2001). Fukazawa et al. (1998) reported that the Si/Fe ratio in the ICM increases with ICM temperature, and Finoguenov et al. (2000) reported that the Si/Fe ratio increases with radius in several clusters. Using Chandra data of groups out to r_{500} , Rasmussen & Ponman (2007) reported that the SNcc contribution increases with radius and completely dominates at r_{500} . XMM-Newton and Suzaku observations have also been used to study the Si/Fe ratio of the ICM in clusters and groups of galaxies. (e.g. Matsushita et al. 2003; Tamura et al. 2004; de Plaa et al. 2007; Rasmussen & Ponman 2007; Matsushita et al. 2007a,b; Sato et al. 2007, 2008; Komiyama et al. 2009; Simionescu et al. 2009; de Grandi & Molendi 2009; Sato et al. 2009a,b, 2010; Sakuma et al. 2011). With Suzaku observations of clusters and groups with ICM temperatures lower than ~ 4 keV, the derived values of Si abundance are close to those of Fe out to $0.2r_{180}$ – $0.3r_{180}$, with a small scatter when using the solar abundance table by Lodders (2003). On the basis of the abundance ratios of Si and Fe, the contributions from SN Ia and SNcc have been estimated. However, excluding cool-core regions, the error bars in the Si/Fe ratio of hotter clusters are very large (Tamura et al. 2004). Matsushita et al. (2012) derived the Si/Fe ratio in the ICM of the Coma cluster from the flux ratios of the Ly α line of H-like Si and the K α line of He-like Fe. The temperature dependence of the line ratio above several keV is relatively small and limits the systematic uncertainty in the derived abundance ra-

tio. The derived Si/Fe ratio of the Coma cluster is approximately 1 solar according to the same solar abundance table, with no radial gradient out to $0.5r_{180}$.

The Perseus cluster is the brightest cool-core cluster with a redshift of 0.018. With Chandra observations, the cool core of the Perseus cluster shows complicated features such as ripples and shocks around radio bubbles (Fabian et al. 2006). With XMM, Tamura et al. (2004) derived the Si/Fe ratio outside the cool core of the Perseus cluster, (50 – $200 h_{100}^{-1}$ kpc), to be 0.77 ± 0.25 in solar units using the solar abundance table by Lodders (2003). Here, the Hubble constant is $H_0 = 100h_{100} \text{ km s}^{-1} \text{ Mpc}^{-1}$. With Suzaku data, Tamura et al. (2009) derived the abundance distribution of Mg, Si, S, Ar, Ca, Cr, Mn, Fe, and Ni of the central region of the Perseus cluster. Simionescu et al. (2011) derived the electron density and Fe abundance profiles out to the virial radius toward the northwest (NW) and east (E) directions observed with Suzaku. Simionescu et al. (2012) studied the large-scale motions of the ICM of the Perseus cluster using ROSAT, XMM, and Suzaku data.

In this paper, we study the Si/Fe and S/Fe ratios in the ICM of the Perseus cluster observed with XMM out to 1.1 Mpc. We collect the K -band luminosity of galaxies and calculated the IMLR and Si-mass-to-light ratios (SMLR) out to this radius. We also calculated the IMLR and constrained SMLR out to 1.8 Mpc, or about the virial radius, using the Suzaku measurements in the NW and E directions by Simionescu et al. (2011). Using a Hubble constant of $70 \text{ km s}^{-1} \text{ Mpc}^{-1}$, $1'$ corresponds to 22 kpc. The value of r_{180} expected from numerical simulations is $r_{180} = 1.95 h_{100}^{-1} \sqrt{k\langle T \rangle / 10 \text{ keV}} \text{ Mpc}$ (Evrard et al. 1996; Markevitch et al. 1998). For the Perseus cluster, this value corresponds to 2.2 Mpc using the average temperature $k\langle T \rangle = 6.1 \text{ keV}$. Hereafter, we denote this radius as $r_{180 < kT >}$. An fit with the universal mass model of Navarro, Frenk and White (NFW) (Navarro et al. 1996, 1997) to the hydrostatic mass derived from the Suzaku observations in the NW direction gave r_{200} (hereafter $r_{200 < \text{He} >}$) as 1.8 Mpc (Simionescu et al. 2011).

We used the solar abundance table by Lodders (2003), in which the solar Si, S and Fe abundances relative to H are 3.47×10^{-5} , 1.55×10^{-5} ,

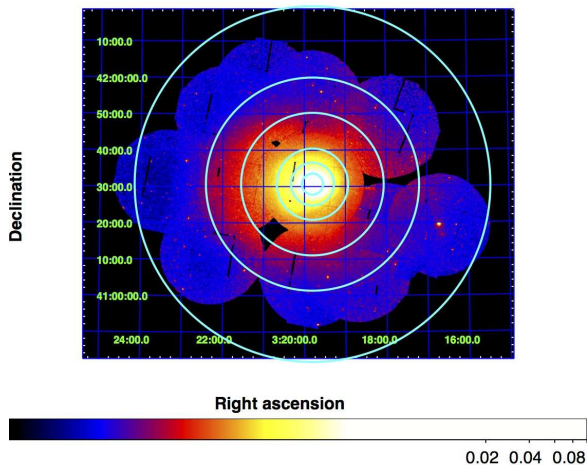


Fig. 1.— Exposure-corrected combined MOS image of the Perseus cluster (0.5–4.0 keV). The circles have radii of 0.03, 0.06, 0.1, 0.2, 0.3, and $0.5r_{180<{\rm kT}}>$. The numbers below the color bar have units of $\text{counts s}^{-1}\text{pixel}^{-1}$.

and 2.95×10^{-5} , respectively, by number. Considering a difference in solar He abundance, the Fe abundance yielded by Lodders (2003) is 1.5 times higher than that using the photospheric value by Anders & Grevesse (1989). Using the table by Lodders (2003), the Si/Fe and S/Fe ratios are factors of 1.55 and 1.52, respectively, smaller than those from Anders & Grevesse (1989).

In this paper, errors were quoted at a 68% confidence level for a single parameter.

2. Observations

We analyzed the archival data of the XMM-Newton observations of the Perseus cluster using PN, MOS1, and MOS2 detectors. In this study, we used SASv12.0, but the details of observations, event selection, and background subtraction are the same as those in Matsushita (2011). The observation log is summarized in Table 1. We included three observations in the archive in addition to those in Matsushita (2011). The exposure-corrected combined MOS image of the Perseus cluster within an energy range of 0.5–4.0 keV is shown in Figure 1. Spectra were accumulated in

concentric annular regions centered on the X-ray peak of the Perseus cluster. The spectra from MOS1 and MOS2 were added.

3. Data Analysis and Results

3.1. Abundance ratios of Si/Fe and S/Fe out to $0.5r_{180<{\rm kT}}>$

Figure 2 shows representative MOS and PN spectra around the Ly α lines of H-like Si and S and K α line of He-like Fe. Although the Si and S lines are clearly seen in the spectra, the peak level of the lines in the spectra is only several percentage points above that of the continuum. For the spectra beyond several hundred kpc, around the Fe line, most of the continuum comes from non-X-ray background (NXB). As a result, a small systematic uncertainty in the response matrix and background can cause a large systematic uncertainty in the abundance of these elements. For example, when we fitted MOS and PN spectra at 0.1 – $0.2r_{180<{\rm kT}}>$ using an energy range of 0.5–10.0 keV with a vAPEC model (Smith et al. 2001), there are discrepancies of a few percent around the Si and S lines between the data and the model and the derived abundances from the PN and MOS detectors differ by a factor of two. When we restricted energy ranges around H-like lines of Si and S and refitted the spectra, the derived abundances strongly depend on the adopted energy range.

To derive the strength of the Si line accurately and to obtain suitable statistics, we fitted the raw (without background subtraction) MOS and PN spectra of each annular region outside 60 kpc ($0.03r_{180<{\rm kT}}>$) out to 1090 kpc ($0.5r_{180<{\rm kT}}>$) simultaneously with a sum of the vAPEC code v2.0.1, two Gaussians for the Ly α line of H-like Si and the K α line of He-like Si, a power-law model with $\Gamma = 1.4$ for the cosmic X-ray background (CXB), and a power-law model that is not folded through the auxiliary response file (ARF) for the NXB. Here, we used an energy range of 1.8–2.1 keV, the Si abundance of the vAPEC model was fixed at 0, and the abundance of the other metals was assumed to have a same value which was left free. Above 1.8 keV, a systematic uncertainty caused by a strong instrumental fluorescence line at ~ 1.7 keV of the MOS detector does not affect the derived Si abundance. To derive S and Fe line strengths, we fitted the spectra in the same

TABLE 1
OBSERVATION LOG OF THE PERSEUS CLUSTER

obsid ^a	(RA, Dec) ^b	Date ^c	Exposures (ks) ^d
0085110101	03 ^h 19 ^m 48.36 ^s +41° 30' 40.6''	2001-01-30	49, 51, 48
0085590201	03 ^h 19 ^m 45.12 ^s +41° 05' 02.5''	2001-02-10	42, 40, 38
0151560101	03 ^h 16 ^m 39.07 ^s +41° 18' 38.5''	2003-02-26	25, 25, 18
0204720101	03 ^h 21 ^m 33.80 ^s +41° 31' 03.1''	2004-02-04	15, 15, 12
0204720201	03 ^h 23 ^m 18.92 ^s +41° 30' 57.2''	2004-02-04	25, 25, 21
0305720301	03 ^h 22 ^m 16.00 ^s +41° 11' 28.0''	2005-08-03	20, 21, 16
0305720101	03 ^h 18 ^m 01.94 ^s +41° 46' 46.2''	2005-09-01	13, 13, 10
0305690101	03 ^h 17 ^m 58.31 ^s +41° 16' 15.7''	2006-02-10	26, 27, 26
0305690301	03 ^h 19 ^m 45.91 ^s +41° 52' 51.0''	2006-02-11	20, 20, 16
0305690401	03 ^h 21 ^m 49.07 ^s +41° 48' 47.2''	2006-02-11	27, 27, 25
0405410101	03 ^h 21 ^m 04.82 ^s +41° 56' 46.7''	2006-08-03	18, 16, 12
0405410201	03 ^h 18 ^m 44.75 ^s +41° 07' 11.2''	2006-08-03	17, 26, 9

^a XMM-Newton observational identifier ^b in J2000.0 ^c Date of start of the observation ^d Exposure times of MOS1, MOS2, and PN, respectively, after screenings

TABLE 2
RESULTS OF THE SPECTRAL FITTING AROUND $K\alpha$ LINE OF Fe

radius (kpc/ $r_{180 < kT >}$)	$F_{6.9}/F_{6.7}$ ^a	kT ^b (keV)	$\chi^2/d.o.f$ ^c	Fe ^d (solar)
60–130/0.03–0.06	0.23 ± 0.01	5.9 ± 0.1	76/93	0.63 ± 0.01
130–220/0.06–0.1	0.30 ± 0.02	6.5 ± 0.2	77/93	0.54 ± 0.03
220–440/0.1–0.2	0.27 ± 0.03	6.2 ± 0.2	128/124	0.47 ± 0.03
440–650/0.2–0.3	0.23 ± 0.05	5.9 ± 0.5	59/52	0.38 ± 0.04
650–1090/0.3–0.5	—	5.6 ± 0.6^e	45/52	0.48 ± 0.07

^a Ratio of flux in units of photons $\text{cm}^{-2}\text{s}^{-1}$ of $\text{Ly}\alpha$ line of H-like Fe and $K\alpha$ line of He-like Fe. ^b The ICM temperature derived from the Fe line ratios using the theoretical expectation by APEC v2.0.1. ^c χ^2 and degrees of freedom of the spectral fitting around the $K\alpha$ line of He-like Fe, or 6.0–7.2 keV. ^d Fe abundance derived from the flux ratio of $K\alpha$ line of He-like Fe and the continuum at 3.5–6.0 keV. ^e ICM temperature derived from the spectral fitting within energy range of 0.8–7.3 keV, considering 10% systematic error.

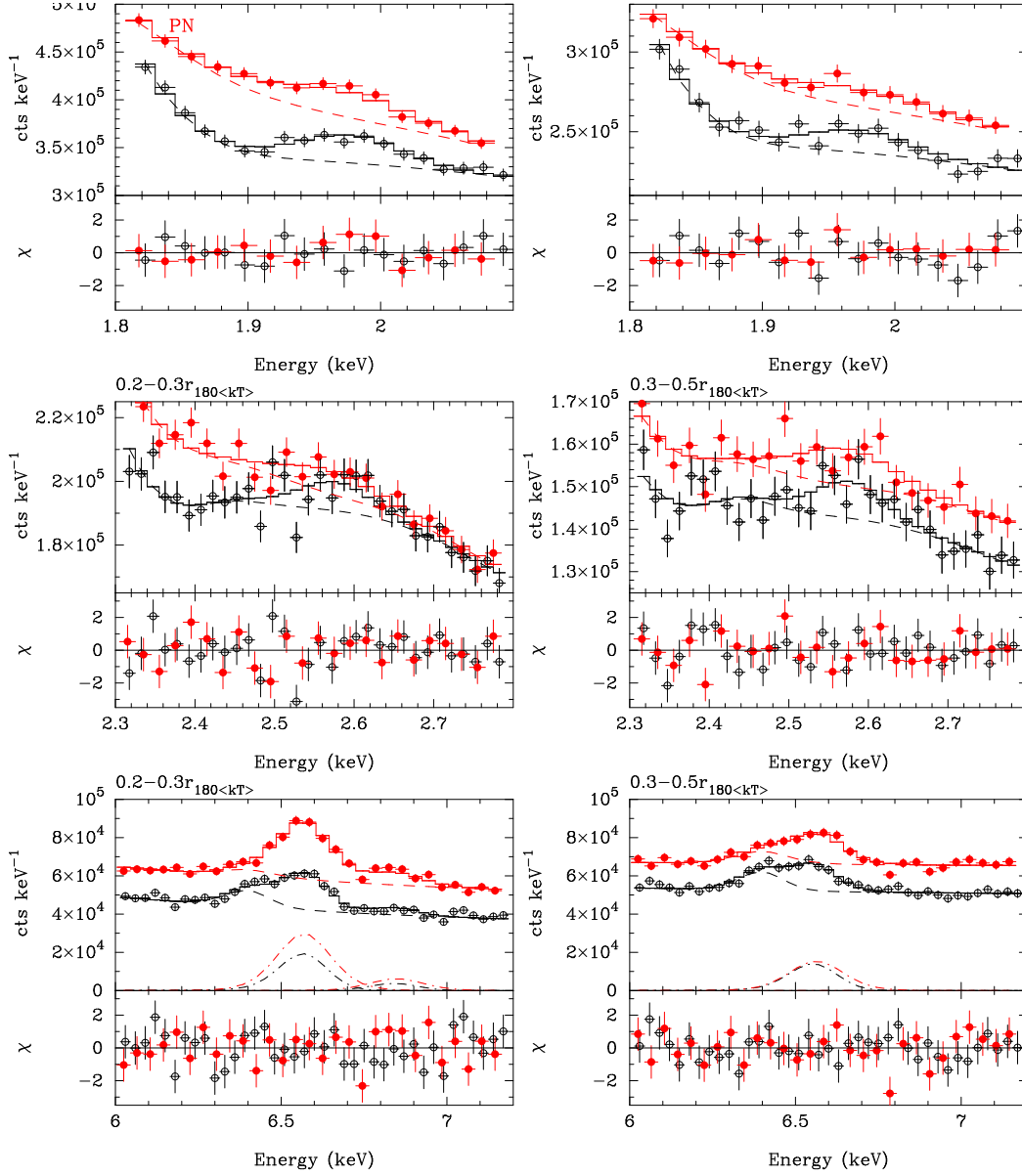


Fig. 2.— Spectra at 440–650 kpc or $0.2-0.3r_{180<KT>}$ (left panels) and 650–1090 kpc or $0.3-0.5r_{180<KT>}$ (right panels) around Ly α lines of H-like Si (top panels) and S (middle panels) and K α line of He-like Fe (bottom panels). Open (black) and closed (red) circles correspond to the MOS and PN spectra, respectively. Here, the background was not subtracted. The solid lines correspond to the best-fit model, which is a sum of a vAPEC v2.0.1 model, Gaussians, and background components. The dashed lines show the contribution of the continuum of the ICM component and the background. The dot-dashed lines in the bottom panels show the contribution of the Fe lines from the ICM. The bump at 6.4 keV in the background component corresponds to an instrumental line.

TABLE 3

LINE RATIOS OF THE $\text{Ly}\alpha$ OF H-LIKE SI AND S TO $\text{K}\alpha$ TO HE-LIKE FE AND Si/Fe AND S/Fe RATIOS.

radius (kpc/ $r_{180 < kT >}$)	$F_{\text{Si}}/F_{\text{Fe}}$ ^a	Si/Fe ^b (solar ratio)	$\chi^2/d.o.f$ ^c	$F_{\text{S}}/F_{\text{Fe}}$ ^a	S/Fe ^b (solar ratio)	$\chi^2/d.o.f$ ^d
60–130/0.03–0.06	0.33 ± 0.03	$0.99^{+0.08}_{-0.08}$	22/22	0.23 ± 0.02	$1.02^{+0.09}_{-0.09}$	80/71
130–220/0.06–0.1	0.27 ± 0.04	$0.87^{+0.14}_{-0.14}$	22/22	0.23 ± 0.03	$1.11^{+0.16}_{-0.16}$	49/71
220–440/0.1–0.2	0.28 ± 0.03	$0.88^{+0.10}_{-0.10}$	16/22	0.17 ± 0.03	$0.76^{+0.14}_{-0.14}$	38/46
440–650/0.2–0.3	0.37 ± 0.05	$1.15^{+0.17}_{-0.19}$	11/22	0.16 ± 0.05	$0.69^{+0.21}_{-0.21}$	54/46
650–1090/0.3–0.5	0.26 ± 0.08	$0.77^{+0.23}_{-0.25}$	19/22	0.22 ± 0.06	$0.97^{+0.26}_{-0.28}$	45/46

^a Ratio of flux in units of photons $\text{cm}^{-2}\text{s}^{-1}$ of $\text{Ly}\alpha$ line of H-like Si or S to $\text{K}\alpha$ line of He-like Fe. ^b The Si/Fe or S/Fe abundance ratios in units of solar ratio derived from the line ratio using the theoretical expectation by APEC v2.0.1. ^c χ^2 and degrees of freedom of the spectral fitting around the $\text{Ly}\alpha$ line of H-like Si, or 1.8–2.1 keV. ^d χ^2 and degrees of freedom of the spectral fitting around the $\text{Ly}\alpha$ line of H-like S, or 2.3–2.8 keV.

manner but used an energy range of 2.3–2.8 keV and 6.0–7.2 keV, respectively. We added a 6.4 keV Gaussian for an instrumental background line. We did not use the region within 60 kpc where the temperature structure is rather complicated because of the cool core (Fabian et al. 2006). Tables 2 and 3 show the results of the spectral fits. We obtained reasonable χ^2 values and, as shown in Figure 2, the spectra around Si, S and Fe lines of the MOS and PN were well reproduced by the model.

Within $0.3r_{180 < kT >}$, we derived the ICM temperature from the line ratio of $\text{Ly}\alpha$ of H-like Fe to $\text{K}\alpha$ of He-like Fe using the APEC v2.0.1 plasma code to reduce systematic uncertainties caused by those in the response matrix and background. At $0.3\text{--}0.5r_{180 < kT >}$, we used deep sky observations as a background, and fitted the background-subtracted spectra within an energy range of 0.8–7.3 keV with an APEC model and a power-law without ARF for a possible remaining NXB component. Furthermore, we added a 10% systematic error in the derived ICM temperature at $0.3\text{--}0.5r_{180 < kT >}$ considering the systematic uncertainties in the response matrix and background (Matsushita 2011). The derived ICM temperatures are shown in Table 2.

Figure 3 shows the ratio of $\text{Ly}\alpha$ of H-like Si or S to the $\text{K}\alpha$ line of He-like Fe plotted against the ICM temperature. The derived line ratios of

Si and S to Fe are close to theoretical expectations at solar Si/Fe and S/Fe ratios, respectively, by APEC v2.0.1 (Figure 3). These two line ratios show a similar temperature dependence: above 5 keV, the line ratios are relatively flat at fixed Si/Fe or S/Fe ratios. The weak temperature dependence can minimize the effect of uncertainties in the temperature structure of the ICM. At a given ICM temperature and abundance ratio, the theoretical expectations obtained by the MEKAL and APEC codes differ by approximately 10 %. The APEC v1.3 code gave almost the same line ratios with APEC v2.0.1. Therefore, any systematic effect due to the plasma codes is expected to be insignificant.

Using the APEC v2.0.1 code, we converted the derived line ratios to the abundance ratio of Si/Fe and S/Fe assuming the single temperature structure. Table 3 and Figure 4 summarize the derived Si/Fe and S/Fe ratios. The derived Si/Fe and S/Fe ratios show no radial gradient out to ~ 1100 kpc, or $0.5r_{180 < kT >}$. Since the temperature dependence of the flux ratio of these lines is relatively flat above several keV, the derived abundance ratios should not change as a result of underestimating the ICM temperature. In contrast, if the ICM temperature is overestimated or if there is an emission component with a lower temperature, the same flux ratio yields a lower ICM abundance. As a result, the Si/Fe and S/Fe

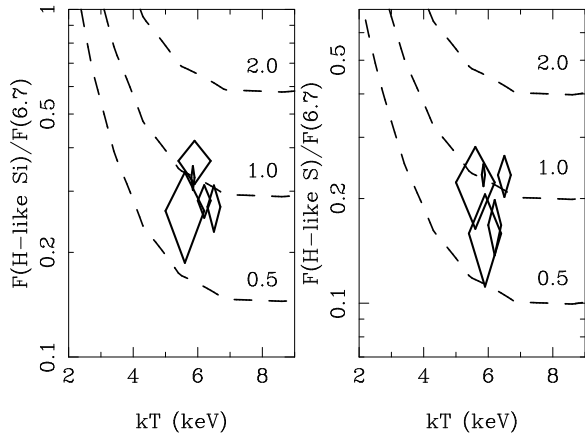


Fig. 3.— Flux ratios of Ly α line of H-like Si (left panel) and S (right panel) to K α line of He-like Fe plotted against plasma temperature. The temperatures and line ratios were derived within the radial ranges listed in Tables 2 and 3. Dashed lines indicate theoretical ratios with a plasma of constant Si/Fe and S/Fe ratios according to APEC v2.0.1 model. The numbers on the plots show the Si/Fe or S/Fe ratios in solar units.

ratios should not be much greater than unity in solar units. The emission-weighted averages of the Si/Fe and S/Fe ratios outside the cool core, 130–1090 kpc, or $0.06\text{--}0.5r_{180< kT >}$ are 0.91 ± 0.08 and 0.93 ± 0.10 , respectively, in units of the solar ratio.

To derive the Fe abundance, we used the flux ratio of the K α line of He-like Fe and the continuum at 3.5–6.0 keV (see Matsushita 2011 for details). Here, we used the APEC v2.0.1 code and the temperatures shown in Table 2. The results are shown in Table 2. The derived Fe abundances are almost the same as in Matsushita (2011). Figure 5 shows the radial profiles of Si, S, and Fe abundances. Beyond 220 kpc ($0.1r_{180< kT >}$) from the center, the Si and S abundances have flat radial profiles at ~ 0.4 solar.

3.2. K-band luminosity of galaxies

Because the K-band luminosity of a galaxy correlates well with the stellar mass, we calculated the luminosity profile of the K-band. We collected K-band magnitudes of galaxies in a $10 \times 10 \text{ deg}^2$ box centered on the center of the Perseus cluster from the Two Micron All Sky Survey (2MASS). Figure 6 shows the galaxies detected by 2MASS.

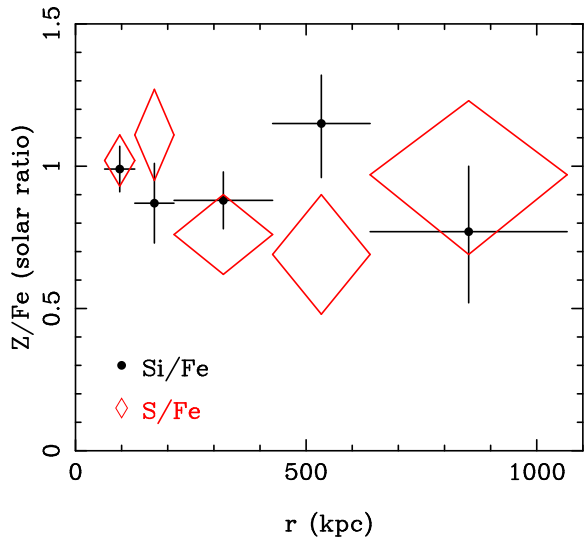


Fig. 4.— Radial profiles of abundance ratios of Si/Fe (closed circles with error bars) and S/Fe (diamonds) in units of solar ratio of the Perseus cluster, derived from flux ratio of Ly α lines of H-like Si or S to K α line of He-like Fe.

In the Perseus cluster, the distribution of galaxies is elongated in an east-west direction. We selected galaxies above the completeness limit of 2MASS, $K_s = 13.5$ in apparent magnitude¹. We corrected the foreground Galactic extinction of $A_K = 0.06$ (Schlegel, Finkbeiner, Davis 1998) by using the NASA/IPAC Extragalactic Database. The K-band surface-brightness profile of the selected galaxies centered on the cD galaxy is shown in Figure 7. The average surface brightness in the region at $1.0r_{180< kT >} < r < 2.0r_{180< kT >}$ ($100' < r < 200'$) was subtracted as the background. Next, we deprojected the brightness profile assuming a spherical symmetry and derived the three-dimensional profile of the K-band luminosity. Figure 8 and Table 4 show the integrated profile of the K-band luminosity. The total K-band luminosity within $r_{180< kT >}$ is relatively insensitive to the background: when we used the region $1.0\text{--}1.5r_{180< kT >}$ as the background, the total K-band luminosity changed by only 10%.

The completeness limit of galaxies of 2MASS corresponds to the absolute K-band magnitude of -21.0 . This value is much fainter than the charac-

¹See <http://www.ipac.caltech.edu/2mass/releases/second/doc/explsup.html>

TABLE 4

CUMULATIVE VALUES OF K -BAND LUMINOSITY (L_K), GAS MASS (M_{gas}), IMLR, AND SMLR DERIVED WITH XMM.

radius (kpc/ $r_{180<KT>}$)	L_K ($10^{12}L_{\odot}$)	M_{gas} ($10^{12}M_{\odot}$)	IMLR ($10^{-4}M_{\odot}/L_{\odot}$)	SMLR ($10^{-4}M_{\odot}/L_{\odot}$)
130/0.06	2.0	3.2	12.5 ± 0.2	7.0 ± 0.1
220/0.1	2.9	6.6	16.0 ± 0.4	8.5 ± 0.2
440/0.2	4.3	21	29 ± 1	15 ± 1
650/0.3	6.0	39	34 ± 2	20 ± 1
1090/0.5	6.9	82	64 ± 5	32 ± 2

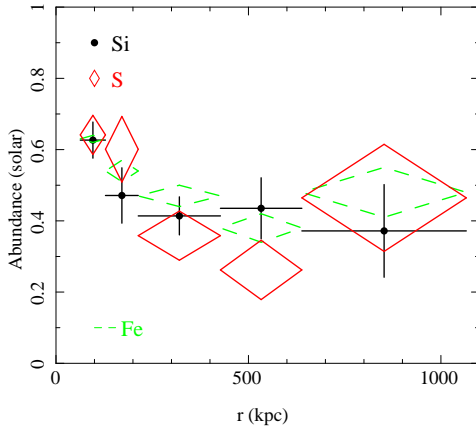


Fig. 5.— Radial profiles of abundances of Si (closed circles with error bars), S (solid diamonds), and Fe (dashed diamonds).

teristic magnitude, M_* of galaxies in the Perseus cluster of -25.09 ± 0.29 (Lin & Mohr 2004). Integrating the luminosity function with the assumption of the Schechter function, the contribution of fainter galaxies below the 2MASS limit is a few %.

3.3. Gas-mass, Si-mass, and Fe-mass profiles

To estimate the integrated gas- and Fe-mass profiles, we accumulated MOS spectra in concentric annular regions with width of $1'-2'$ out to $50'$, or $0.5r_{180<KT>}$. We subtracted those of deep sky observations accumulated over the same detector regions as background. We fitted these spectra within an energy range of 1.6–5.0 keV with an

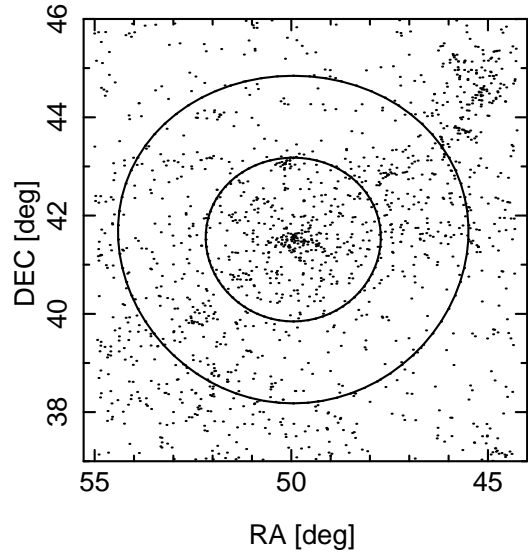


Fig. 6.— Distribution of galaxies detected by 2MASS in the K -band. The circles correspond to 1.0 and $2.0r_{180<KT>}$.

APEC model to avoid uncertainties in the background. Here, the temperature and Fe abundance were restricted within the error bars shown in Table 2. We fitted the radial profile of the derived emission measures from the spectral fits per area with a sum of two β -models. The profile is well represented with the model and we calculated the electron density profile. We integrated the electron density profiles observed with XMM in this way out to $0.5r_{180<KT>}$ and Suzaku toward E and NW directions by Simionescu et al. (2011) out to $\sim r_{200<HE>}$ and derived the in-

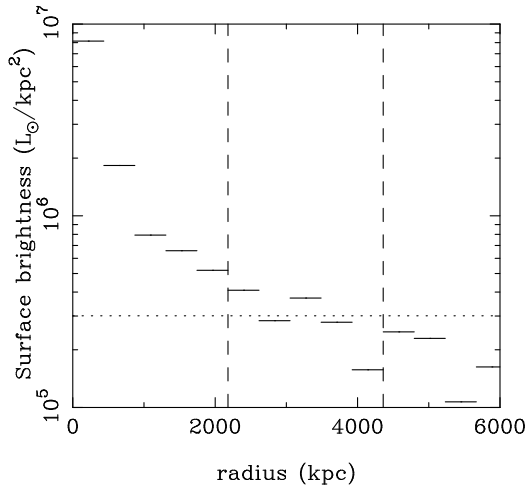


Fig. 7.— Surface brightness profile of galaxies around the Perseus cluster observed with 2MASS photometric data in the K -band. Dashed lines correspond to $1.0r_{180<KT>}$ and $2.0r_{180<KT>}$. The dotted line shows the adopted background level.

egrated gas-mass profiles (Figure 8 and Table 4). Because of gas sloshing and cold front at 700 kpc in the E direction, the integrated gas mass toward this direction is higher than that of the NW direction. The gas-mass profile with XMM falls between the profiles of the two directions with Suzaku out to $0.5r_{180<KT>}$. With the integrated K -band luminosity and gas mass profiles with XMM and weighted average for the two directions with Suzaku, we calculated the radial profiles of cumulative gas-mass-to-light ratio. In spite of differences in the observed azimuthal directions and in the analysis methods, as shown in Figure 9, the Suzaku and XMM gave similar radial profiles for the gas-mass-to-light ratio. The ratio increases with radius out to the virial radius.

We used the Si and Fe abundance profiles from XMM-Newton data and derived integrated mass profiles of Fe and Si in the ICM. We also integrated the Fe mass using the weighted average of the Fe abundance profiles for the E and NW directions observed with Suzaku (Simionescu et al. 2011). The radial profiles of the cumulative IMLR and SMLR are shown in Figure 10 and Table 4. The error bars of the mass-to-light ratio include only the errors in abundance. These profiles continue to increase with radius out to 1800 kpc, ~

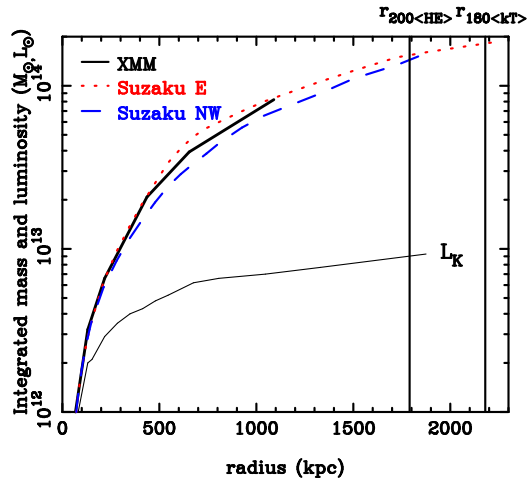


Fig. 8.— Integrated K -band luminosity (thin solid line) and gas-mass profiles of the Perseus cluster derived with XMM-Newton (bold solid line), and Suzaku (E:red dotted line, NW: blue dashed line), integrated over the electron density profiles, assuming spherical symmetry. The two vertical lines show $r_{180<KT>}$ and $r_{200<HE>}$.

$r_{200<HE>}$.

4. Discussions

4.1. The abundance pattern and contribution of SN Ia and SNcc

The derived Si/Fe and S/Fe ratios in the ICM of the Perseus cluster show no radial gradient out to 1.1 Mpc, or $0.5r_{180<KT>}$. The emission-weighted averages of the Si/Fe and S/Fe ratios within 0.06 – $0.5r_{180<KT>}$ are 0.91 ± 0.08 and 0.93 ± 0.10 , respectively, in solar units. These values are consistent with the emission-weighted average of the Si/Fe ratio of 0.99 ± 0.13 in solar units of the Coma cluster within $0.5r_{180<KT>}$. They are also consistent with the values of ~ 0.8 in solar units of those in clusters and groups observed with Suzaku with ICM temperature less than several keV (e.g. Matsushita et al. 2007a; Sato et al. 2007, 2008, 2009a,b, 2010; Komiyama et al. 2009; Sakuma et al. 2011).

Based on the abundance ratios including Si and Fe, the contribution from SN Ia and SNcc were derived (e.g. Finoguenov et al. 2000; de Plaa et al. 2007; Rasmussen & Ponman 2007; Sato et al.

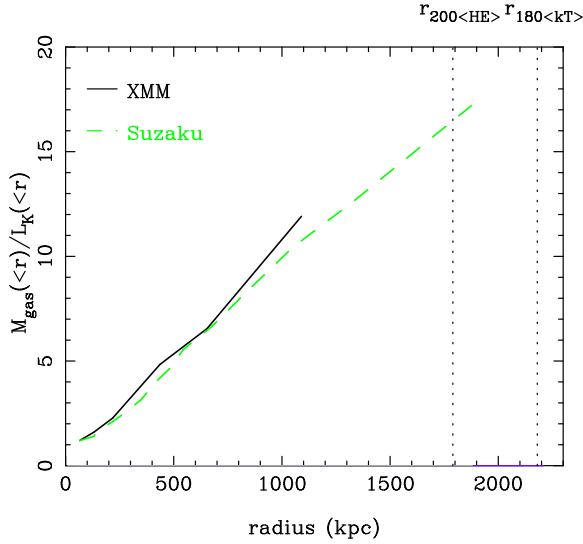


Fig. 9.— Radial profiles of integrated gas-mass-to-light ratio with XMM (solid line) and Suzaku (dashed line). Here, we used the weighted average of the E and NW results of Suzaku.

2007; de Grandi & Molendi 2009; Simionescu et al. 2009; Matsushita et al. 2012). Since Si and Fe were synthesized by both SN Ia and SNcc, the contribution of the two types of SN strongly depends on the adopted nucleosynthesis model of SN Ia. With the yields of SNcc with metallicity = 0.02 by Nomoto et al. (2006), they found that by using the classical deflagration model, W7 (Iwamoto et al. 1999), and a delayed detonation (DD) model, WDD3 (Iwamoto et al. 1999), for the theoretical SN Ia yield, over a half of the Fe and a few tens of percent of Si in the ICM were synthesized in SN Ia. By adopting another DD model, WDD1 (Iwamoto et al. 1999), they found that approximately half of the Si and most of the Fe come from SN Ia. Suzaku enabled us to measure O and Mg abundances in the ICM outside cool cores of clusters and groups of galaxies with ICM temperatures smaller than several keV. Sato et al. (2007, 2009a, 2010) found that the mixture of yields of the W7 model and SNcc gave better fits of the observed abundance pattern of O, Mg, Si, S, and Fe in the ICM observed with Suzaku than for the WDD1 model and SNcc. The number ratio of SNcc and SN Ia to synthesize metals in the ICM was also estimated with Suzaku and XMM data (e.g. de Plaa et al. 2007; de Grandi & Molendi

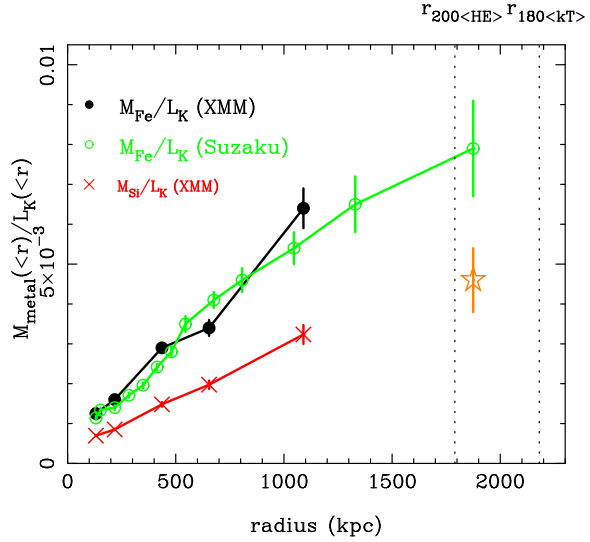


Fig. 10.— Radial profiles of IMLR with XMM (black closed circles) and Suzaku (green open circles) and SMLR with XMM (red crosses). Here, we used the weighted average of the E and NW results of Suzaku and assumed spherical symmetry. The orange star indicates the SMLR assuming the Si/Fe ratio beyond $0.5r_{180<KT>}$ is 0.91 ± 0.08 in solar units.

2009; Simionescu et al. 2009; Sato et al. 2007, 2009a, 2010). Using the Suzaku results including O and Mg, the number ratio of SNcc to SN Ia was estimated to be ~ 3.5 and ~ 2 , using the W7 and WDD1 models, respectively.

We also calculated yields mixtures of nucleosynthesis models. By adopting a Si/Fe ratio of 0.91 ± 0.08 in solar units in the ICM of the Perseus cluster, and using the W7 model, we find that 65–74 % and 23–30 % of Fe and Si, respectively, were synthesized by SN Ia. Using the WDD1 model, 80–91 % and 56–75 % of Fe and Si, respectively, originated from SN Ia. Here, we also used the yields of SNcc with metallicity = 0.02 by Nomoto et al. (2006). The difference in the Si/Fe ratios in the yields of SNcc assuming a Salpeter initial mass function (IMF) and a top-heavy IMF and different nucleosynthesis models by Chieffi & Limongi (2004) and Woosley & Weaver (1995) are relatively small, within $\sim 10\%$.

From the Si/Fe ratio of the Perseus cluster, we also derived the number ratio of the SNcc to SN Ia to contribute metals in the ICM. Using the W7

and WDD1 models, the derived number ratios are 3.2–4.8 and 0.8–2.0, respectively. The number ratio from the Si/Fe ratio strongly depends on the adopted nucleosynthesis model, as found by previous studies.

The average S/Si ratio of the ICM in the Perseus cluster is 1.02 ± 0.14 in solar units. The S/Fe ratio of the theoretical yield of SNcc by Nomoto et al. (2006) with metallicity = 0.02 and the Salpeter IMF is 0.83 in solar units. The yields of the W7 model and the WDD models are approximately 1.1–1.2 in solar units. Therefore, the observed S/Si ratio of the Perseus cluster is consistent with the yields of both SN Ia and SNcc.

4.2. Si-Mass-to-Light Ratios and initial mass function of stars

The integrated SMLR using the K -band at $0.5r_{180<K>}$ of the Perseus cluster is $\sim 0.003 M_{\odot}/L_{K,\odot}$. When we assume that the Si/Fe ratio beyond $0.5r_{180<K>}$ is the same as that within the radius, the SMLR out to $0.86r_{180<K>}$ becomes $0.004\text{--}0.005 M_{\odot}/L_{K,\odot}$ (Figure 10). The Si abundance is not expected to increase with radius, because gas is more extended than stars. Then, assuming the Si abundance beyond $0.5r_{180}$ is 0.4 solar, which is the Si abundance at $0.1\text{--}0.5r_{180}$, the SMLR becomes $0.005 M_{\odot}/L_{K,\odot}$. If the clumping of the gas is significant (Simionescu et al. 2011) and the gas fraction at the virial radius is close to the value of the Wilkinson Microwave Anisotropy Probe (WMAP) 7 (Komatsu et al. 2011), the cumulative SMLR out to $0.86r_{180<K>}$ is overestimated by 20–30%. To summarize, the expected value of the SMLR at $0.86 r_{180<K>}$, is $0.003\text{--}0.005 M_{\odot}/L_{K,\odot}$. Adopting the W7 and WDD1 models for the SN Ia nucleosynthesis model, the SMLR synthesized by SNcc becomes $0.002\text{--}0.004 M_{\odot}/L_{K,\odot}$ and $0.001\text{--}0.002 M_{\odot}/L_{K,\odot}$, respectively.

The O, Mg, and Si abundances in the hot interstellar medium (ISM) in early-type galaxies reflect stellar metallicity because the ISM is thought to come from stellar mass loss. The abundances of these elements in the hot ISM in bright early-type galaxies observed with Suzaku are approximately 0.5–2 solar (Konami et al. 2012). Extrapolating the observed gradient of the Mg index in optical spectra of elliptical galaxies, Kobayashi & Arimoto (1999) calculated that

the mean stellar metallicity, $[\text{Fe}/\text{H}]$ of individual galaxies ranges from -0.8 to $+0.3$ and correlates with stellar luminosity. They also found that typical $[\text{Mg}/\text{Fe}]$ is approximately $+0.2$. These results indicate that the Si abundance in stars in giant cluster galaxies is approximately 0.5–2 solar. Using K -band, the stellar mass-to-light ratio in bright early-type galaxies are approximately unity (Nagino & Matsushita 2009). As a result, the SMLR trapped in stars should be $0.0005\text{--}0.002 M_{\odot}/L_{K,\odot}$. The estimated value of the total SMLR in the Perseus cluster (i.e., the sum of the SMLR in the ICM and in stars) is $0.004\text{--}0.008 M_{\odot}/L_{K,\odot}$.

Theoretical models predict that the oxygen-mass-to-light ratio (OMLR) and SMLR of a cluster are very sensitive functions of the slope of the IMF (Renzini 2005). Here, the oxygen and silicon mass are a sum of that trapped in stars and that in the ICM. Adopting a Salpeter IMF with a slope of 2.35, and difference in the stellar mass-to-light ratio between the B-band and K -band equal 5, we find that the expected value of the SMLR from SNcc is $\sim 0.002 M_{\odot}/L_{K,\odot}$. This value is close to the sum of the SMLR in stars and ICM from SNcc, adopting the nucleosynthesis yield of WDD1 model. Using the W7 yields, the SMLR from SNcc corresponds to a slope of ~ 2 based on the calculation by Renzini (2005). A top-heavy IMF with a slope of 1.35 overproduces metals more than that with a factor of 20. Therefore, the expected value of the SMLR out to the virial radius does not need the top-heavy IMF.

4.3. Fe mass and past SN Ia rate

The solar Si/Fe abundance ratio in the ICM of the Perseus cluster indicates that most of the Fe was synthesized by SN Ia. The estimated rate of the current SN Ia rate in present early-type galaxies are $0.1\text{--}0.3 \text{ SN Ia}/(100 \text{ yr})/(10^{10} L_{B,\odot})$ (Cappellaro et al. 1997, 1999; Turatto et al. 1999; Sharon et al. 2007; Mannucci et al. 2008). We adopted the Fe mass per SN Ia rate by W7 model of $0.75 M_{\odot}$ (Iwamoto et al. 1999) and $L_K/L_B \sim 5 L_{K,\odot}/L_{B,\odot}$ for early-type galaxies (Nagino & Matsushita 2009). Then, accumulating the present SN Ia rate over the Hubble time, 13.7 Gyr, the expected IMLR from the SN Ia becomes $(2\text{--}6) \times 10^{-4} M_{\odot}/L_{K,\odot}$. This value is over an order of magnitude smaller than the

observed IMLR $(6-7) \times 10^{-3} M_{\odot}/L_{K,\odot}$ and $(7-9) \times 10^{-3} M_{\odot}/L_{K,\odot}$ within $0.5 r_{180<KT>}$ and $\sim 0.86 r_{180<KT>}$, respectively.

The increase of the radial profile of the IMLR with radius of clusters indicates that Fe in the ICM extends farther than stars, at least out to $0.5 r_{180<KT>}$. Leccardi & Molendi (2008) and Matsushita (2011) discovered that the Fe abundance profiles of the ICM within r_{500} are flatter than expected from the numerical simulations by Fabjan et al. (2008), without AGN feedback. These results indicate that a significant fraction of Fe is synthesized in an early phase of cluster evolution, because if metal enrichment occurs after the formation of clusters, the metal distribution is expected to follow the stellar distribution. Considering that most Fe is synthesized by SN Ia, the lifetimes of most of SN Ia are much shorter than the Hubble time, and the SN Ia rate in cluster galaxies was much higher in the past. If the IMF is close to that in our Galaxy and if most of stars in our Galaxy and clusters were already formed before a few Gyrs ago, the abundance pattern (including the ICM and stars in cluster galaxies) should naturally be similar to the solar abundance pattern.

4.4. Comparison of radial profiles of IMLR with other systems

Figure 11 compares the cumulative IMLR profile of the Perseus cluster with that of clusters of galaxies observed with Suzaku or XMM out to $0.5-1.0 r_{180<KT>}$ including Coma (8 keV; Matsushita et al. 2012), Abell 262 (2 keV; Sato et al. 2009b), AWM 7 (3.6 keV; Sato et al. 2008), and the Hydra A (3.0 keV; Sato et al. 2012) clusters. The IMLR profiles of three cool-core clusters at a similar redshift, Abell 262, AWM 7, and the Perseus cluster agree very well with each other at $0.2-0.5 r_{180<KT>}$, whereas the Coma cluster has a lower IMLR at $0.5 r_{180<KT>}$. There is no significant temperature dependence on the derived IMLR profiles. Since the IMLR profiles increase with radius, comparison of the total IMLR values requires observations of IMLR profiles of clusters out to the virial radii.

At a given radius in units of $r_{180<KT>}$, the Hydra A cluster has a factor-of-two-higher IMLR than the Perseus cluster. Because of the higher redshift of the Hydra A cluster and lower ICM temperature, the number of galaxies detected in

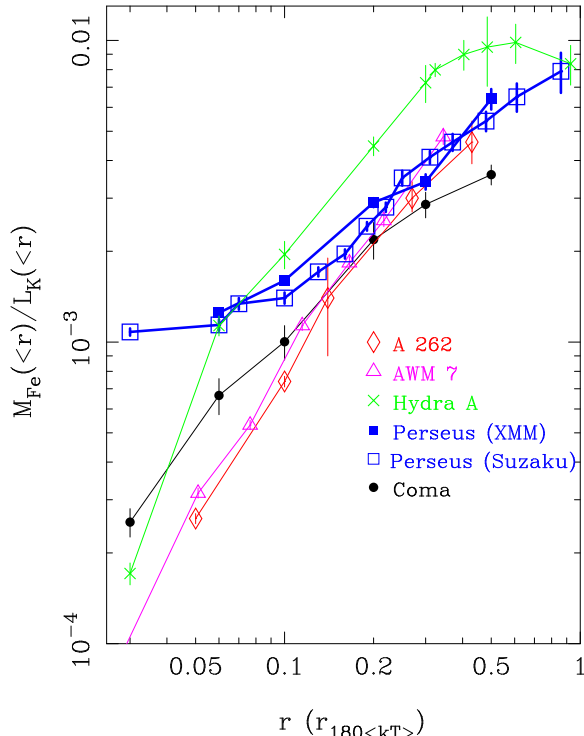


Fig. 11.— Profiles of IMLR plotted against radius scaled with $r_{180<KT>}$ of the Perseus cluster (closed squares with XMM and open squares with Suzaku), AWM 7 (open triangles, Sato et al. (2008), Sato et al. in preparation), Abell 262 (open diamonds, Sato et al. (2009b)), Hydra A cluster (crosses, Sato et al. (2012)) and the Coma cluster (closed circles, Matsushita et al. (2012)).

Hydra A might not be sufficient to deprojected the luminosity profiles in K -band. However, at $\sim r_{180<KT>}$, where systematic uncertainties due to the limited number of galaxies are relatively small, the cumulative IMLR of the Hydra A and the Perseus clusters agree well. No systematic dependence on the ICM temperature is evident for these two clusters with temperatures of 3 keV and 6 keV.

At the center, within $0.1 r_{180<KT>}$, the Perseus cluster and the Hydra A have much higher IMLR than the other systems, which is due to the very bright cool core of these two clusters. Within this radius, the cD galaxies dominate the K -band luminosity and the systematic uncertainties in the K -band luminosity should be small. The IMLR

within $0.1 r_{180<KT>}$ of the Perseus and Hydra A clusters are about $1.5\text{--}2 \times 10^{-3} M_{\odot}/L_{K,\odot}$, which is a factor 3–10 higher than the expected IMLR from SN Ia assuming the present SN Ia rate over the Hubble time. The higher IMLR in these two clusters reflect higher gas-mass-to-light ratio in $0.1 r_{180<KT>}$, since the Fe abundance of these two clusters are not higher than those of the other clusters in this region (Simionescu et al. 2009; Matsushita 2011). Simionescu et al. (2009) measured the distribution of O, Si, S, Ar, Ca, Fe and Ni in the ICM of the Hydra A cluster within $\sim 0.1 r_{180<KT>}$. They found O abundance decreases with radius and amount of metals are much higher than the expected values by stellar winds. They discussed the initial enrichment by SNcc in the early phase in cluster evolution and mixing of these metals. The O/Fe and Mg/Fe ratios within the cool core of the Perseus cluster are about unity in solar units (Matsushita & Tamura 2011) and agrees with the O/Fe ratio in the cool core of the Hydra A cluster (Simionescu et al. 2009). The metals already synthesized in the protocluster phase can dominate those in the central regions of these two clusters.

4.5. Gas-mass-to-light ratio

The integrated gas mass to light ratio of the Perseus cluster increases with radius out to 1800 kpc, or $\sim r_{200<HE>}$. At 1800 kpc, $M_{\text{gas}}(< r)/L_K(< r) = 16 M_{\odot}/L_{\odot}$. This value is not so different from $21 \pm 4 M_{\odot}/L_{\odot}$ for the Hydra A cluster ($< kT > = 3$ keV) at $r_{200<HE>}$. The stellar and gas mass fractions within r_{500} depend on the total system mass (Lin, Mohr, Stanford 2003; Lin & Mohr 2004; Sun et al. 2009; Giodini et al. 2009; Zhang et al. 2010). The gas density profiles in the central regions of groups and poor clusters were observed to be shallower than those obtained by the self-similar model, and the relative entropy level was correspondingly higher than that in rich clusters (Ponman, Cannon, Navarro 1999; Ponman, Sanderson, Finoguenov 2003; Sun et al. 2009). Then, the difference in the ratio of gas mass to stellar mass might reflect differences in distributions of gas and stars, which reflects the history of energy injection from galaxies into the ICM. To study the fractions of stars and gas in clusters of galaxies, and their dependence on the system mass, measurements beyond r_{500} of other

clusters are required.

Based on the Suzaku observations of the NW and E directions of the Perseus cluster, Simionescu et al. (2011) proposed that the gas-clumping effect is significant beyond r_{500} , and that the electron density is overestimated. As a result, M_{gas} within $r_{200<HE>}$ is overestimated by a factor of 1.3–1.5. Adopting this value for the gas mass, the gas-mass-to-light ratio at $r_{200<HE>}$ becomes 11–12 M_{\odot}/L_{\odot} , which is close to the value at 1000 kpc, or $0.6 r_{200<HE>}$. In other words, if there is a significant clumping effect, the gas-mass-to-light ratio becomes flat beyond this radius out to $r_{200<HE>}$.

5. Summary and Conclusion

We analyzed XMM-Newton data of the Perseus cluster out to $0.5r_{180<KT>}$ and derived the Si/Fe and S/Fe ratios in the ICM from the flux ratios of the Ly α lines of H-like Si and S to the K α line of He-like Fe. The small temperature dependence of the line ratio limits the systematic uncertainty in the derived abundance ratio. The derived Si/Fe and S/Fe ratios in the ICM show no radial gradient. The emission-weighted averages of the Si/Fe and S/Fe ratios beyond the cool core of the Perseus cluster are 0.91 ± 0.08 and 0.93 ± 0.10 , respectively, in solar units. These abundance ratios indicate that most of Fe in the ICM within $0.5r_{180<KT>}$ was synthesized by SN Ia.

We collected *K*-band luminosities in galaxies detected with 2MASS and derived the cumulative radial profile of the *K*-band luminosity of stars in the Perseus cluster. We calculated the cumulative IMLR and SMLR profiles out to $r_{180<KT>}$. Furthermore, by using the electron density profiles and Fe abundance profiles in the two directions observed with Suzaku, we calculated the cumulative IMLR profile out to the virial radius. We also constrained the SMLR value out to this radius. The SMLR of the Perseus cluster out to the virial radius is significantly smaller than expected from the top-heavy IMF, which has a slope of 1.35, and is more consistent of a slope of the Salpeter IMF. With the present SN Ia rate, the IMLR within the virial radius is an order-of-magnitude higher than the SN Ia yield accumulated over the Hubble time. Since the IMLR increases with radius, the most of Fe from SN Ia were synthesized in an early-phase

of cluster formation.

REFERENCES

- Anders, E., & Grevesse, N., 1989, *Geochim. Cosmochim. Acta*, 53, 197
- Arnaud, M., Rothenflug, R., Boulade, O., Vigroux, L., & Vangioni-Flam, E. 1992, *A&A*, 254, 49
- Cappellaro, E., Turatto, M., Tsvetkov, D. Y., Bartunov, O. S., Pollas, C., Evans, R., & Hamuy, M. 1997, *A&A*, 322, 431
- Cappellaro, E., Evans, R., & Turatto, M. 1999, *A&A*, 351, 459
- Chieffi, A., & Limongi, M. 2004, *ApJ*, 608, 405
- de Grandi, S., & Molendi, S. 2009, *A&A*, 508, 565
- de Plaa, J., Werner, N., Bleeker, J. A. M., et al. 2007, *A&A*, 465, 345
- Evrard, August E., Metzler, Christopher A. & Navarro, Julio F. 1996, *ApJ*, 469, 494
- Fabian, A. C., Sanders, J. S., Taylor, G. B., et al. 2006, *MNRAS*, 366, 417
- Fabjan, D., Tornatore, L., Borgani, S., Saro, A., & Dolag, K. 2008, *MNRAS*, 386, 1265
- Finoguenov, A., David, L. P. & Ponman, T. J. 2000, *ApJ*, 544, 188
- Finoguenov, A., Arnaud, M. & David, L. P. 2001, *ApJ*, 555, 191
- Fukazawa, Y., Makishima, K., Tamura, T., Ezawa, H., Xu, H., Ikebe, Y., Kikuchi, K. & Ohashi, T. 1998, *PASJ*, 50, 187
- Fukazawa, Y., Makishima, K., Tamura, T., Nakazawa, K., Ezawa, H., Ikebe, Y., Kikuchi, K. & Ohashi, T. 2000, *MNRAS*, 313, 21
- Fujita, Y., Tawa, N., Hayashida, K., et al. 2008, *PASJ*, 60, 343
- Giodini, S., et al. 2009, *ApJ*, 703, 982
- Iwamoto, K., Brachwitz, F., Nomoto, K., Kishimoto, N., Umeda, H., Hix, W. R., & Thielemann, F.-K. 1999, *ApJS*, 125, 439
- Kobayashi, C., & Arimoto, N. 1999, *ApJ*, 527, 573
- Komatsu, E., Smith, K. M., Dunkley, J., et al. 2011, *ApJS*, 192, 18
- Komiyama, M., Sato, K., Nagino, R., Ohashi, T. & Matsushita, K. 2009, *PASJ*, 61, 337
- Konami, S. Matsushita, K., Nagino, R., and Tamagawa, T. submitted to *ApJ*
- Leccardi, A. & Molendi, S. 2008, *A&A*, 487, 461
- Lin, Y.-T., Mohr, J. J., & Stanford, S. A. 2003, *ApJ*, 591, 749
- Lin, L. T., & Mohr, J., J. 2004, *ApJ*, 617, 879
- Lodders, K. 2003, *ApJ*, 591, 1220
- Makishima, K. et al. 2001, *PASJ*, 53, 401
- Mannucci, F., Maoz, D., Sharon, K., Botticella, M. T., Della Valle, M., Gal-Yam, A., & Panagia, N. 2008, *MNRAS*, 383, 1121
- Markevitch, M., Forman, W. R., Sarazin, C. L. & Vikhlinin, A. 1998, *ApJ*, 503, 77
- Matsushita, K., Finoguenov, A. & Böhringer, H. 2003, *A&A*, 401, 443
- Matsushita, K. et al. 2007a, *PASJ*, 59, 327
- Matsushita, K., Böhringer, H., Takahashi, I. & Ikebe, Y., 2007b, *A&A*, 462, 953
- Matsushita, K. 2011, *A&A*, 527, A134
- Matsushita, K., Sato, T., Sakuma, E., & Sato, K., 2012, *PASJ* in press, arXiv:1208.609
- Matsushita, K. & Tamura, T. 2011, submitted to *A&A*
- Nagino, R., & Matsushita, K. 2009, *A&A*, 501, 157
- Navarro, J. F., Frenk, C. S., & White, S. D. M. 1996, *ApJ*, 462, 563
- Navarro, J. F., Frenk, C. S., & White, S. D. M. 1997, *ApJ*, 490, 493
- Nomoto, K., Tominaga, N., Umeda, H., Kobayashi, C., & Maeda, K. 2006, *Nuclear Physics A*, 777, 424

- Ponman, T. J., Cannon, D. B., & Navarro, J. F. 1999, *Nature*, 397, 135
- Ponman, T. J., Sanderson, A. J. R., & Finoguenov, A. 2003, *MNRAS*, 343, 331
- Rasmussen, J., & Ponman, T. J. 2007, *MNRAS*, 380, 1554
- Rasmussen, J., & Ponman, T. J. 2009, *MNRAS*, 399, 239
- Renzini, A., Ciotti, L., D’Ercole, A., & Pellegrini, S. 1993, *ApJ*, 419, 52
- Renzini, A. 2005, *The Initial Mass Function 50 Years Later*, Edited by E. Corbelli and F. Palle, INAF Osservatorio Astrofisico di Arcetri, Firenze, Italy; H. Zinnecker, *Astrophysikalisches Potsdam, Germany. Astrophysics and Space Science Library Volume 327*. Published by Springer, Dordrecht, 2005, p.221
- Sakuma, E., Ota, N., Sato, K., Sato, T., & Matsushita, K. 2011, *PASJ*, 63, 979
- Sato, K., Tokoi, K., Matsushita, K., Ishisaki, Y., Yamasaki, N. Y., Ishida, M. & Ohashi, T. 2007b, *ApJ*, 667, 41
- Sato, K., Matsushita, K., Ishisaki, Y., Yamasaki, N. Y., Ishida, M., Sasaki, S. & Ohashi, T. 2008, *PASJ*, 60, 333
- Sato, K., Matsushita, K., Ishisaki, Y., Yamasaki, N. Y., Ishida, M. & Ohashi, T. 2009a, *PASJ*, 61, 353
- Sato, K., Matsushita, K. & Gastaldello, F. 2009b, *PASJ*, 61, 365
- Sato, K., Kawaharada, M., Nakazawa, K., Matsushita, K., Ishisaki, Y., Yamasaki, N. Y. & Ohashi, T. 2010, *PASJ*, 62, 1445
- Sato, T., Sasaki, T., Matsushita, K., et al. 2012, *PASJ*, 64, 95
- Sharon, K., Gal-Yam, A., Maoz, D., Filippenko, A. V., & Guhathakurta, P. 2007, *ApJ*, 660, 1165
- Schelegel, D. J., Finkbeiner, D. P., & Davis, M. 1998, *ApJ*, 500, 525
- Simionescu, A., Werner, N., Böhringer, H., Kaastra, J. S., Finoguenov, A., Brüggen, M. & Nulsen, P. E. J. 2009, *A&A*, 493, 409
- Simionescu, A., et al. 2011, *Science*, 331, 1576
- Simionescu, A., Werner, N., Urban, O., et al. 2012, *ApJ*, 757, 182
- Smith, R. K., Brickhouse, N. S., Liedahl, D. A., & Raymond, J. C. 2001, *ApJ*, 556, L91
- Sun, M., Voit, G. M., Donahue, M., Jones, C., Forman, W., & Vikhlinin, A. 2009, *ApJ*, 693, 1142
- Tamura, T., Kaastra, J. S., den Herder, J. W. A., Bleeker, J. A. M., & Peterson, J. R. 2004, *A&A*, 420, 135
- Tamura, T., Maeda, Y., Mitsuda, K., et al. 2009, *ApJ*, 705, L62
- Tsuru, T., 1992, PhD thesis, University of Tokyo
- Turatto, M., Cappellaro, E., & Petrosian, A. R. 1999, *Activity in Galaxies and Related Phenomena*, 194, 364
- Woosley, S. E., & Weaver, T. A. 1995, *ApJS*, 101, 181
- Zhang, Y.-Y., Okabe, N., Finoguenov, A., et al. 2010, *ApJ*, 711, 1033